Enrichment of Jupiter's Atmosphere by Late Planetesimal Bombardment

Sho Shibata [ID] and Ravit Helled [ID]
Institute for Computational Science (ICS), University of Zurich, Switzerland; s.shibata423@gmail.com

Abstract

Jupiter's atmosphere is enriched with heavy elements by a factor of about 3 compared to a protosolar composition. The origin of this enrichment and whether it represents the bulk composition of the planetary envelope remain unknown. Internal structure models of Jupiter suggest that its envelope is separated from the deep interior and that the planet is not fully mixed. This implies that Jupiter's atmosphere was enriched with heavy elements just before the end of its formation. Such enrichment can be a result of late planetesimal accretion. However, in situ Jupiter formation models suggest a decreasing accretion rate with increasing planetary mass, which cannot explain Jupiter's atmospheric enrichment. In this study, we model Jupiter's formation and show that the migration of proto-Jupiter from ∼20 au to its current location can lead to late planetesimal accretion and atmospheric enrichment. Late planetesimal accretion does not occur if proto-Jupiter migrates only a few astronomical units. We suggest that if Jupiter's outermost layer is fully mixed and is relatively thin (up to ∼20% of its mass), such late accretion can explain its measured atmospheric composition. It is therefore possible that Jupiter underwent significant orbital migration followed by late planetesimal accretion.

Unified Astronomy Thesaurus concepts: Planet formation (1241); Planetary atmospheres (1244); Planetary interior (1248); Planetary migration (2206); Planetesimals (1259); Jupiter (873); Atmospheric composition (2120)

1. Introduction

The Galileo probe measured the elemental abundances in Jupiter's atmosphere and found that several heavy elements are enriched by a factor of ∼3 compared to a protosolar composition (e.g., Owen et al. 1999; Wong et al. 2004; Atreya et al. 2020). Also, the recent measurement of Jupiter's water abundance by Juno implies that oxygen is enriched by a factor of a few (Li et al. 2020).

The origin of the heavy-element enrichment of Jupiter's atmosphere remains unknown, and several ideas have been suggested to explain this enrichment. One idea is that the atmospheric enrichment is caused by the erosion of a primordial heavy-element core (e.g., Stevenson 1982; Guillot et al. 2004; Bosman et al. 2019; Öberg & Wordsworth 2019). However, in this case, the materials dissolved into the deep interior must be mixed by convection and be delivered to the upper envelope. Because recent structure models of Jupiter imply that the planet is not fully convective (e.g., Leconte & Chabrier 2013; Wahl et al. 2017; Vazan et al. 2018; Debras & Chabrier 2019), the validity of this explanation is questionable and should be investigated in detail. Alternatively, Jupiter's atmospheric enrichment could be a result of the accretion of enriched disk gas (Guillot et al. 2006; Bosman et al. 2019; Schneider & Bitsch 2021). However, this scenario cannot reproduce the atmospheric enrichment of water and refractory materials (Schneider & Bitsch 2021). Finally, it is possible that Jupiter's atmosphere has been enriched by the late accretion of heavy elements in the form of planetesimal accretion, as we explore in this work.

Previous investigations of Jupiter's formation considered planetesimal accretion in the context of in situ formation where proto-Jupiter grows at 5.2 au (e.g., Zhou & Lin 2007; Shiraishi

& Ida 2008; Shibata & Ikoma 2019; Podolak et al. 2020; Venturini & Helled 2020). In this case, as the gas accretion rate increases, the planetesimal accretion rate decreases. Therefore, if Jupiter is not fully convective, the enrichment of its outer envelope is difficult to explain because the accreted planetesimals are mainly deposited in the deep interior and not delivered to the upper envelope. However, there is a clear theoretical indication that planets migrate (e.g., Bitsch et al. 2015; Ida et al. 2018; Kanagawa et al. 2018; Bitsch et al. 2019; Tanaka et al. 2020). During the planetary migration, planetesimals can be captured by the planet (e.g., Alibert et al. 2005), and it was recently shown that the migration rate regulates the planetesimal accretion rate (Shibata et al. 2020, 2021; Turrini et al. 2021). It was shown in Shibata et al. (2021) that rapid planetesimal accretion occurs in the limited region that we refer to as the "sweet spot for planetesimal accretion" (SSP). The SSP is located around ≲10 au for planets smaller than Jupiter, suggesting that proto-Jupiter enters the SSP after a large fraction of its envelope has already accumulated. If this is the case, a nonnegligible amount of planetesimals can be accreted into the outer layer of the proto-Jupiter and lead to an enrichment of its atmosphere.

In this Letter, we simulate Jupiter's formation including planetary migration and investigate the accretion rate of planetesimals. In Section 2, we describe our numerical model and the formation pathways of proto-Jupiter we consider. Our results are presented in Section 3, where we show that rapid planetesimal accretion occurs just before the end of Jupiter formation. A discussion on the connection to Jupiter's measured atmospheric metallicity is presented in Section 4. Finally, our conclusions are discussed in Section 5.

2. Methods

We perform orbital integration calculations of planetesimals around a protoplanet growing via disk gas accretion (increasing planetary mass M_p) and migrating inward due to tidal
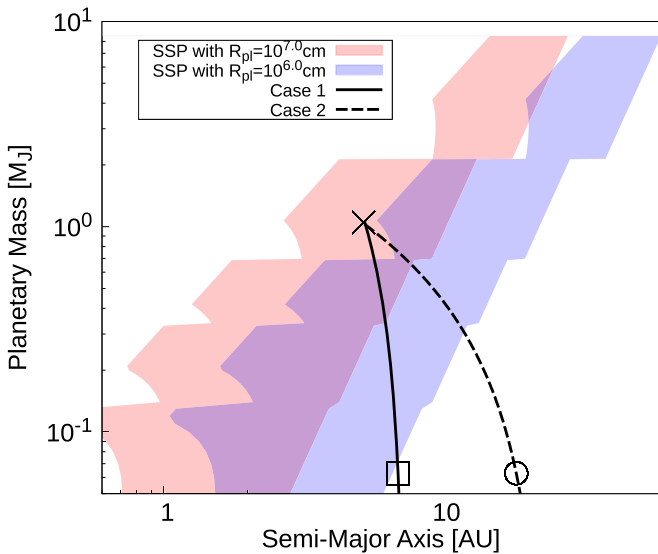
Figure 1. Orbital evolution pathways used in our model. Solid and dashed lines show the evolution pathways in Case 1 and Case 2, respectively. The square and circle are the core formation locations for Case 1 and Case 2, respectively. The cross corresponds to Jupiter. The red and blue areas show the sweet spot for planetesimal accretion (SSP) (Shibata et al. 2021) with $R_{\rm pl} = 10^{7.0}$ cm and $R_{\rm pl} = 10^{6.0}$ cm, respectively.

interaction with the surrounding gaseous disk (decreasing planetary semimajor axis $a_{\rm p}$). Our simulations begin from the rapid gas accretion phase for a given planetary mass $M_{\rm p,0}$ and semimajor axis $a_{\rm p,0}$. We assume that there are many single-sized planetesimals with a radius of $R_{\rm pl}$ around the protoplanet's orbit. The protoplanet then encounters these planetesimals and can capture some of them. Planetesimals are represented by test particles and are therefore only affected by the gravitational forces from the central star (with a mass of $M_{\rm s} = M_\odot$) and the protoplanet, as well as the drag force of the gaseous disk. To model the drag force, we follow the model of Adachi et al. (1976). The dynamical integration for the bodies is performed using the numerical framework presented in Shibata & Ikoma (2019).

We adapt the formation model of Tanaka et al. (2020), where both the gas accretion timescale $\tau_{\rm acc}$ and planetary migration timescale $\tau_{\rm tide}$ depend on the gap structure opened by the protoplanet's tidal torque. In this model, the effect of the density profile of the disk is canceled, and the relation between the two timescales is given by

$$\frac{\tau_{\rm tide}}{\tau_{\rm acc}} = \left| \frac{d \ln M_{\rm p}}{d \ln a_{\rm p}} \right| = \left(\frac{M_{\rm p}}{M_{\rm th}} \right)^{-2/3}, \qquad (1)$$

where $M_{\rm th}$ is the threshold mass determined by the gas accretion and migration models. In Tanaka et al. (2020), $M_{\rm th}$ is estimated as $\sim 10^{-2} M_{\rm s}$. Their gas accretion model assumed that most of the disk gas entering the hill sphere is accreted by the planet. However, as pointed in Ida et al. (2018), recent hydrodynamic simulations clearly show that this is an overestimate of the gas accretion rate (e.g., Szulágyi et al. 2016; Kurokawa & Tanigawa 2018). We therefore consider two formation pathways with $M_{\rm th} = 10^{-2} M_{\rm s}$ (Case 1) and $M_{\rm th} = 10^{-3} M_{\rm s}$ (Case 2). Figure 1 shows the formation pathways of proto-Jupiter for these two cases where the solid and dashed lines correspond to Case 1 and Case 2, respectively.

We set $M_{\rm p,0} = 6 \times 10^{-5} M_\odot \sim 20 M_\oplus$ and adjust $a_{\rm p,0}$ to be 6.9au for Case 1 (square point) and 18.3au for Case 2 (circle point) in order to ensure that the protoplanet reaches Jupiter's mass at its current location (cross in Figure 1). It is clear that other formation paths are possible; however, in this study we focus only on two typical cases representing short and long migration in order to investigate how they compare in terms of late heavy-element enrichment.

The SSP is determined by the planetary migration rate and the damping rate of the planetesimal's orbit due to disk gas drag. Therefore, the location of the SSP depends on various parameters, such as the disk viscosity, aspect ratio, and planetesimal size (Shibata et al. 2021). In order to investigate the effect of the SSP, we consider different planetesimal sizes $R_{\rm pl}$. In Figure 1, we plot the formation pathways of the protoplanet and the SSP when considering two different planetesimal sizes. As we show below, the relative position between the formation pathways and the SSP affects the enrichment of the planetary envelope. The detailed model and other parameters used in our simulations are presented in Appendix A.

3. Results

Figure 2 shows the results of our simulations. The upper panels present the cumulative captured mass of planetesimals $M_{\rm cap}$ as a function of calculation time $t - t_0$. In Case 1 (left panel), the cumulative captured mass gradually increases with time although the accretion rate decreases. This is because the expanding speed of the feeding zone decreases with the increase in gas accretion timescale and planetary mass (Shibata & Ikoma 2019). This results in the depletion of planetesimals inside the feeding zone. For Case 2 (right panel), the accretion rate decreases until $t - t_0 \lesssim 10^6$ yr. Planetesimal accretion nearly stops when $t - t_0 \sim 10^5$ yr. However, a second planetesimal accretion phase occurs before the end of Jupiter's formation. As shown in Figure 1, proto-Jupiter enters the SSP before the end of its formation, which triggers the second phase of planetesimal accretion. Before it enters the SSP, many planetesimals are shepherded by the mean motion resonances. This leads to a large number of planetesimals that enter the feeding zone when proto-Jupiter reaches the SSP.

The planetesimal accretion rate increases with decreasing $R_{\rm pl}$. This is because the SSP moves outward with decreasing $R_{\rm pl}$, and the length of the evolutionary pathway that overlaps with the SSP is longer for smaller planetesimals. On the other hand, the initiation of the second phase of planetesimal accretion occurs earlier for smaller planetesimals because proto-Jupiter enters the SSP earlier.

The lower panels of Figure 2 show the heavy-element distribution formed in the Jupiter envelope $Z_{\rm p}$ by the end of the simulations. To estimate $Z_{\rm p}$, we assume that the captured planetesimals are deposited in the outer regions at that time and ignore any mixing processes, namely $Z_{\rm p}$ is obtained from the planetesimal accretion rate normalized by the mass growth rate $\dot{M}_{\rm cap}/\dot{M}_{\rm p}$. For Case 1 (left panel), the planetesimal accretion rate decreases with time and the outer envelope is barely enriched with planetesimals. On the other hand, for Case 2 (right panel), the planetesimals accreted during the second accretion phase are deposited in the outer envelope ($\gtrsim 0.5 M_{\rm J}$). This is most profound for $R_{\rm pl} = 10^{6.5}$, where the metallicity of Jupiter's atmosphere can be enhanced by a factor of a few. It
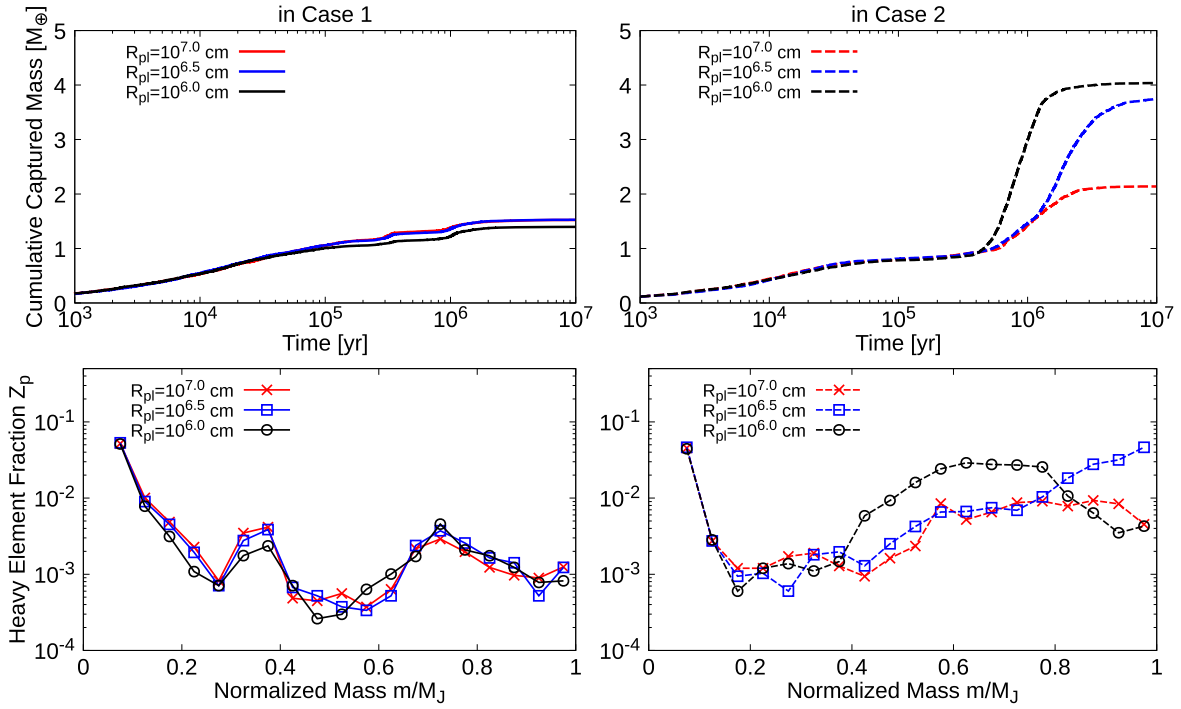
Figure 2. Upper panels: the cumulative captured mass of planetesimals as a function of calculation time $t - t_0$ in Case 1 (left) and in Case 2 (right). The different colors correspond to the different sizes of planetesimals. The planetesimal accretion rate decreases with time in Case 1; however, a second rapid planetesimal accretion occurs before the end of its formation in Case 2. Lower panels: the heavy-element mass fraction Z_p that formed in Jupiter's envelope as a function of the normalized mass m/M_p. The bin's width is set to be $0.05\ m/M_J$. Planetesimals accreted during the second accretion phase are deposited into the outer envelope.

should be noted, however, that the final metallicity of Jupiter's atmosphere would depend on the mixing and settling of the heavy elements accreted at this late stage. We discuss this topic in more detail in Section 4.

It should be noted that in this study we focus on the enrichment of Jupiter's atmosphere. However, formation models should also reproduce the total heavy-element mass in the planet. Interior models of Jupiter that fit Juno gravity data suggest that Jupiter's interior is enriched with a few tens of $M_\oplus$ of heavy elements although the exact heavy-element mass is not well constrained. In this study, we begin the simulation of proto-Jupiter with a mass of $\sim$20 $M_\oplus$ of heavy elements without specifying the formation process of the heavy-element core. Core formation via planetesimal/pebble accretion is expected to lead to deep interiors that are heavy-element dominated in composition and for the buildup of composition gradients (e.g., Helled & Stevenson 2017; Lozovsky et al. 2017; Valletta & Helled 2020). We therefore assume that the deep interior of the forming planet consists of mostly heavy elements.

4. Discussion

4.1. Enrichment of Jupiter's Atmosphere

The accreted heavy elements can be redistributed by the mixing processes in Jupiter's envelope that can occur over a timescale of gigayears. Here, for simplicity, we assume that the uppermost layer of Jupiter's envelope with mass $M_{conv,top}$ is separated from the deeper interior and that the accreted heavy-element mass deposited in this region $M_{cap,top}$ is uniformly distributed. In other words, we assume that the outermost region of Jupiter's envelope is convective and homogeneously mixed and that the envelope below this layer has a different composition. This assumption is in fact consistent with recent
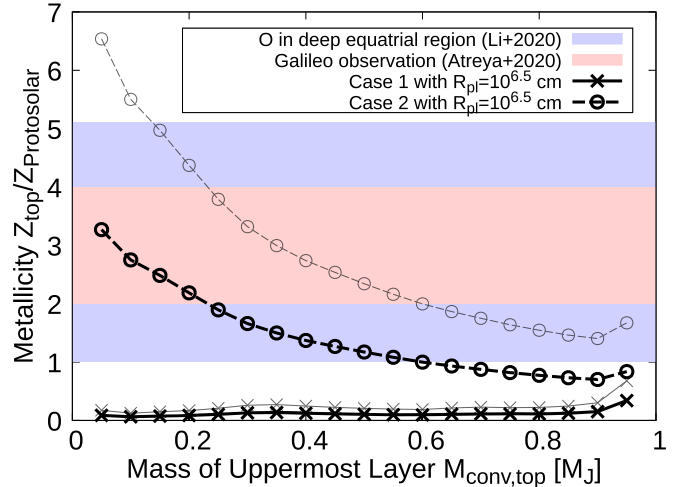
Figure 3. Metallicity of the uppermost layer Z_{top} as a function of the mass of the uppermost layer $M_{conv,top}$. The metallicity is normalized by the protosolar metallicity $Z_{protosolar}$. We adopt 0.0142, obtained in Asplund et al. (2009), to be consistent with our disk model. The blue and red areas show the oxygen abundance retrieved by Juno ($2.7^{+2.4}_{-1.7}$; Li et al. 2020) and the atmospheric composition suggested by Galileo (2–4; Atreya et al. 2020). Solid and dashed lines show the results in Case 1 and Case 2, respectively. Here, we show the cases of $R_{pl} = 10^{6.5}$ cm. We also plot the cases where the planetesimal disk is twice heavier than the disk in our model with thin lines.

models of Jupiter's interior (e.g., Vazan et al. 2018). In this case, the metallicity of Jupiter's atmosphere (outer envelope) Z_{top} is given by

$$Z_{top} = \frac{M_{cap,top}}{M_{conv,top}}. \qquad (2)$$

Figure 3 shows Z_{top} as a function of $M_{conv,top}$. The solid and dashed black lines correspond to Case 1 and Case 2,

respectively. Here, we show the cases of $R_{pl} = 10^{6.5}$ cm with which the most efficient atmospheric enrichment is achieved. The thin lines show the results for the cases where we use a planetesimal disk that is twice more massive than our baseline model. In Case 1, Z_{top} is significantly lower than protosolar metallicity independently of $M_{conv,top}$. This is because the total mass of accreted planetesimals is smaller than 1 $M_\oplus$ and the planetesimals are accreted at early stages and are deposited in the deep interior. Even when we consider a planetesimal disk that is several times more massive, it is difficult to explain Jupiter's enriched atmosphere in Case 2.

On the other hand, for Case 2, several $M_\oplus$ of heavy elements are accreted during the late phases of Jupiter's formation leading to the enrichment of the planetary uppermost envelope as we show in Figure 3. We find that in this case Z_{top} is enhanced in comparison to protosolar metallicity for $M_{conv,top} \lesssim 0.6 M_J$. The blue and red areas correspond to the measured water abundance by Juno (Li et al. 2020) and the elemental abundance measured by the Galileo probe (Atreya et al. 2020), respectively. We find that Jupiter's atmospheric metallicity can be explained with $M_{conv,top} \lesssim 0.2 M_J$. The maximum required value of $M_{conv,top}$ can increase when considering larger sizes of the planetesimal disk. It should be noted, however, that the size of the uppermost convective envelope of Jupiter is not well constrained and changes with different structure models (e.g., Wahl et al. 2017; Vazan et al. 2018; Debras & Chabrier 2019). Using a planetary evolution model, Vazan et al. (2018) found that a primordial composition gradient in the deep interior can be partially eroded by convective mixing, leading to a large convective envelope (60% of Jupiter mass) for Jupiter today. In this case, a more massive planetesimal disk, as well as smaller planetesimals and/or larger planetary capture radius that could increase the heavy-element accretion efficiency (see Appendix A), is required to reproduce the measured elemental abundances in Jupiter's atmosphere. To explain Jupiter's atmospheric enrichment, our results clearly favor a small outer convective layer for Jupiter as proposed by Debras & Chabrier (2019) ($M_{conv,top} \sim 0.1 M_J$).

4.2. Very Volatile Materials

The measurement of the Galileo probe also finds that very volatile materials are also enriched in Jupiter's atmosphere. Such elements are expected to condense in a cold environment where the temperature is $\lesssim 30$ K (Atreya et al. 2020). Figure 4 shows the accreted heavy-element mass as a function of the initial semimajor axis of the planetesimals. The mass of accreted planetesimals when $M_p > 0.8 M_J$ is indicated by meshed textures. In Case 2, the planetesimals accreted onto the upper envelope mainly come from the relatively cold outer region of the disk (10 to $\sim$15 au). However, even for the case of an optically thick disk (Sasselov & Lecar 2000), the midplane temperature is too high for very volatile materials, such as N_2 and Ar, to condense into planetesimals. It is also possible that Jupiter migrated from a larger radial distance, such as >30 au (e.g., Bitsch et al. 2015, 2019). However, the migration of a core from several tens of astronomical units to 5 au requires rapid formation of the core at these large distances, and it is still unclear whether a core can form in such outer disk in timescales that are significantly shorter than the disk's lifetime. Additional processes could help in enriching the atmosphere, for example, by decreasing the local midplane
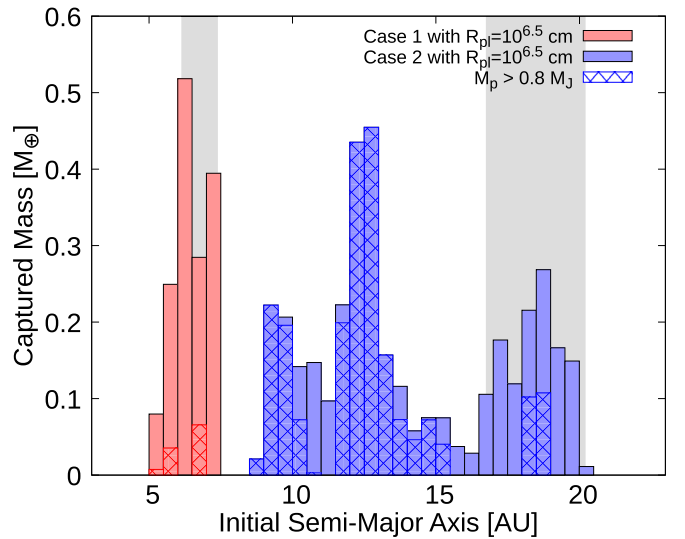

Figure 4. Mass of captured planetesimals as a function of the initial semimajor axis of planetesimals. Red and blue correspond to Case 1 and Case 2, respectively. The meshed textures show the mass of the captured planetesimals when $M_p > 0.8 M_J$. Here we show the cases of $R_{pl} = 10^{6.5}$ cm. Bin width is set to 0.5 au. The gray filled areas show the initial feeding zones of proto-Jupiter.

temperature with a shadow of the inner disk (e.g., Ohno & Ueda 2021) or by increasing the metallicity of the accreting disk gas toward the end of disk depletion (Guillot & Hueso 2006). Also, volatiles must keep being condensed during the accretion process, which might be unrealistic given the expected heating by proto-Jupiter's luminosity (Barnett & Ciesla 2022) or ablation by the disk gas drag (e.g., Eriksson et al. 2021). The accretion of volatile materials by Jupiter should be investigated in detail in future research.

4.3. Assumed Disk Model

In this study, we adopt a relatively large disk in comparison to observed protoplanetary disks (e.g., Andrews et al. 2010). The planetesimal accretion rate is expected to change when considering different disk models. However, as long as Jupiter's formation pathway overlaps with the SSP, the second planetesimal accretion is expected to occur. To confirm that this is indeed the case, we performed additional simulations considering different disk models. The results are presented in Appendix B. Indeed, we find that a late phase of planetesimal accretion always occurs when proto-Jupiter enters the SSP. We therefore conclude that the occurrence of a second planetesimal accretion by proto-Jupiter is robust.

In this study, we assumed that the planetesimals are homogeneously distributed. However, recent planetesimal formation models imply that planetesimals are distributed in a ring-like structure around ice lines because the solid-to-gas ratio is locally enhanced due to the pileup of solid materials (Armitage et al. 2016; Drążkowska & Alibert 2017; Hyodo et al. 2021). Ice lines of volatile materials such as CO_2 could lead to planetesimal formation at $\sim$10–15 au. In addition, the disk temperature evolution is important to consider in planetesimal formation models around ice lines (e.g., Lichtenberg et al. 2021). We hope to investigate other planetesimal distributions and their time evolution in future studies. Finally, it should be noted that the initial planetesimal distribution also affects the leftover distribution of small objects. By the end of the simulations in Case 2, more than $10 M_\oplus$ of planetesimals
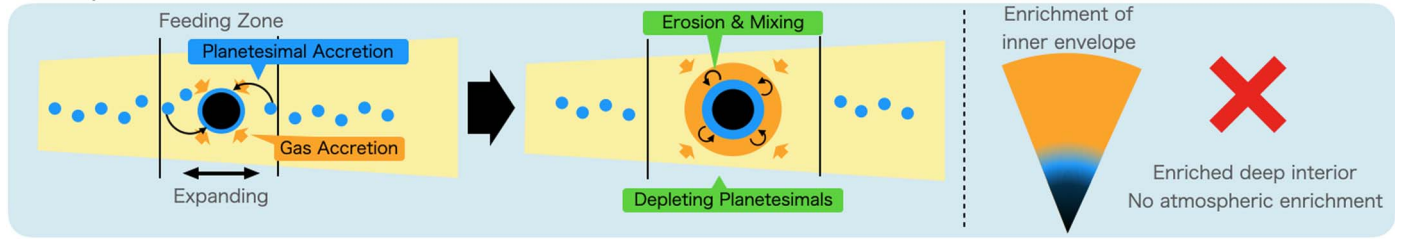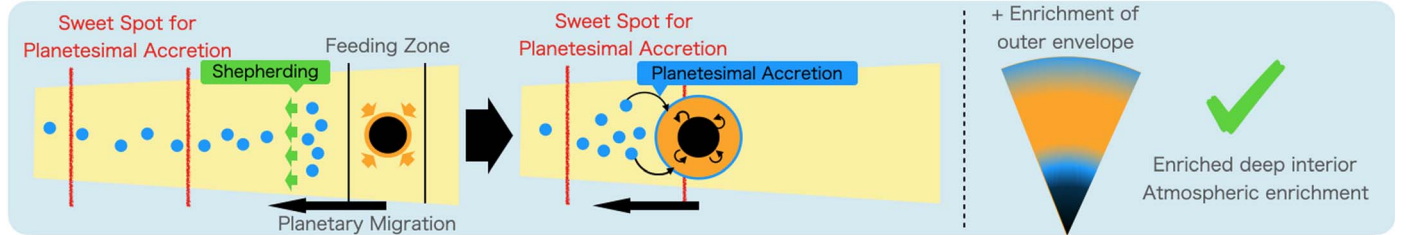
Figure 5. Sketch for planetesimal accretion and the forming composition gradient in Jupiter envelope. The above panel shows the case when proto-Jupiter migrates from 7 to 5 au. Infalling gas covers the envelope enriched via planetesimal accretion and only the inner region of the Jupiter envelope is enriched with heavy elements. The bottom panel shows the case when proto-Jupiter migrates from 20 to 5 au. If the protoplanet reaches the sweet spot for accretion just before the end of gas accretion, planetesimals are deposited into the outer envelope. A several-times-enriched Jupiter atmosphere can be formed if the size of the outermost convective layer is as small as $\lesssim 0.2 M_{\rm J}$.

remain in the region interior to Jupiter's orbit. These objects do not exist at present in the solar system; however, the nonaccreted planetesimals mainly come from distances $\lesssim 10$ au. Therefore, if the planetesimals were formed around 10–15 au, the number of planetesimals shepherded into the region interior to Jupiter's orbit would be reduced. In addition, it is known that long-term dynamical evolution and gravitational interactions with other giant planets can lead to the loss of planetesimals around Jupiter's orbit (Dones et al. 2004; O'Brien et al. 2007). The orbital evolution of planetesimals after Jupiter's formation should be investigated in future work.

5. Conclusions

We investigated Jupiter's origin, focusing on the possibility of planetesimal accretion toward the end of its formation. We considered two formation pathways: Case 1, where proto-Jupiter migrates from ~ 7 au to its current location, and Case 2, where proto-Jupiter migrates from ~ 20 au. For Case 1, we find that the planetesimal accretion rate decreases with increasing planetary mass. Therefore, in this case, Jupiter's outer envelope cannot be enriched with heavy elements. On the other hand, in Case 2, we find that a late planetesimal accretion phase occurs before the end of Jupiter's formation. This happens because proto-Jupiter enters the SSP (see the text for details), which leads to an enrichment of Jupiter's atmosphere.

The accreted heavy elements are expected to mix and redistribute in Jupiter's envelope during its long-term evolution. Assuming the mass of the uppermost layer of Jupiter's envelope $M_{\rm conv,top}$ and deposited heavy materials fully mixing, we find that:

1. Jupiter's atmosphere is barely enriched in Case 1 regardless of the size of $M_{\rm conv,top}$.
2. A relatively thin layer of $M_{\rm conv,top} \lesssim 0.2 M_{\rm J}$ in Case 2 is consistent with the observed metallicity of Jupiter's atmosphere.

The results of the two formation models we consider and their outcomes are summarized in the sketches of Figure 5.

To conclude, we suggest that Jupiter's core was formed via pebble accretion and had migrated from ~ 20 au to its current location followed by a late phase of planetesimal accretion that enriches its atmosphere with heavy elements. In this scenario, we infer an internal structure that is (at least qualitatively) consistent with interior models of Jupiter in which the outermost part of Jupiter's envelope is enriched with heavy elements by a factor of a few relative to the protosolar composition. In our scenario, the atmospheric enrichment is a result of late planetesimal accretion and not due to convective mixing of heavy elements from the deep interior, as suggested by other studies (e.g., Bosman et al. 2019; Öberg & Wordsworth 2019). We conclude that Jupiter's atmosphere can be enriched with heavy elements if proto-Jupiter had migrated from ~ 20 au to its current location. Further studies on the convection of Jupiter's envelope and the mixing of heavy materials should be used for constraints on Jupiter's formation pathway.

Appendix A
Planetary Formation Model

We describe the formation model used in this study, which is based on the model by Tanaka et al. (2020). We adopt the planetary migration model with a shallow gap empirically obtained by Kanagawa et al. (2018). The migration rate is given by

$$\frac{dr_{\rm p}}{dt} = -2c \frac{M_{\rm p}}{M_{\rm s}} \frac{r_{\rm p}^2 \Sigma_{\rm gap}}{M_{\rm s}} \left(\frac{h_{\rm p}}{r_{\rm p}}\right)^{-2} v_{\rm K,p}, \qquad (A1)$$

where c is the constant set as $c = 3$ in this study, $r_{\rm p}$ is the orbital radius of the planet, $\Sigma_{\rm gap}$ is the surface density of disk gas at the gap bottom, $h_{\rm p}$ is the disk gas scale height, and $v_{\rm K,p}$ is the Kepler velocity of the planet. During the late formation stage of

gas-giant planets, the gas accretion rate is regulated by the gas flow around the protoplanet rather than the cooling rate of the planetary envelope. In this case, the gas accretion rate is given by Tanigawa & Watanabe (2002):

$$\frac{dM_p}{dt} = D\Sigma_{gap},\qquad(A2)$$

with

$$D = 0.29\left(\frac{M_p}{M_s}\right)^{4/3}\left(\frac{h_p}{r_p}\right)^{-2} r_p^2\Omega_p,\qquad(A3)$$

where Ω_p is the Kepler angular velocity of the planet. Using Equation (A1) and Equation (A2), we can obtain Equation (1) and $M_{th} = 10^{-2}$. In Case 2, to account for the lower accretion rate, we artificially reduce the gas accretion rate by a factor of $\sim$5 and obtain $M_{th} = 10^{-3}$.

Our baseline disk model is based on the self-similar solution for the surface density profile of disk gas (Lynden-Bell & Pringle 1974). The midplane temperature of disk gas T_{disk} is given by

$$T_{disk} = 280K\left(\frac{r}{1au}\right)^{-1/2},\qquad(A4)$$

where r is the radial distance from the central star. In this case, the disk gas viscosity $\nu = \alpha_{vis}c_sh_s$, where α_{vis} is the viscosity parameter (Shakura & Sunyaev 1973) and c_s is the sound speed of disk gas and is proportional to r, and the self-similar solution Σ_{SS} is given as

$$\Sigma_{SS} = \frac{M_{tot,0}}{2\pi R_d^2}\left(\frac{r}{R_d}\right)^{-1} T^{-3/2}\exp\left(-\frac{r}{TR_d}\right),\qquad(A5)$$

with

$$T = 1 + \frac{t}{\tau_{vis}},\qquad(A6)$$

$$\tau_{vis} = \frac{R_d^2}{\nu_d},\qquad(A7)$$

where $M_{tot,0}$ is the disk total mass at $t = 0$, R_d is the radial scaling length of the protoplanetary disk, τ_{vis} is the characteristic viscous timescale, and ν_d is a disk gas viscosity at $r = R_d$. The surface density profile of disk gas is altered by the gap opening around the planet, the gas accretion onto the planet, and the disk depletion. We include these effects, and the surface density profile of disk gas Σ_{gas} is given by

$$\Sigma_{gas} = f_{gap}f_{acc}f_{dep}\Sigma_{SS},\qquad(A8)$$

where f_{gap} is the gap-opening factor, f_{acc} is the gas accretion factor, and f_{dep} is the disk depletion factor. For the gap-opening factor, we adapt the empirically obtained model by Kanagawa et al. (2017). The gap structure changes with the radial distance from the planet $\Delta r = |r - r_p|/r_p$, and f_{gap} is written as a function of Δr as

$$f_{gap} = \begin{cases} \dfrac{1}{1 + 0.04K} & \text{for } \Delta r < \Delta R_1, \\ 4.0K'^{-1/4}\Delta r - 0.32 & \text{for } \Delta R_1 < \Delta r < \Delta R_2, \\ 1 & \text{for } \Delta R_2 < \Delta r, \end{cases}\qquad(A9)$$

with

$$K = \left(\frac{M_p}{M_s}\right)^2\left(\frac{h_p}{r_p}\right)^{-5}\alpha_{vis}^{-1},\qquad(A10)$$

$$K' = \left(\frac{M_p}{M_s}\right)^2\left(\frac{h_p}{r_p}\right)^{-3}\alpha_{vis}^{-1},\qquad(A11)$$

$$\Delta R_1 = \left\{\frac{1}{4(1 + 0.04K)} + 0.08\right\}K'^{1/4},\qquad(A12)$$

$$\Delta R_2 = 0.33K'^{1/4}.\qquad(A13)$$

In the disk region closer in than the planet, the disk surface density is reduced by the gas accretion onto the planet. When the gas accretion rate is given by Equation (A2) and the gap structure is given by Equation (A9), f_{acc} is written as (Tanaka et al. 2020)

$$f_{acc} = \begin{cases} 1 & \text{for } r > r_p \\ \left\{1 + \dfrac{D}{3\pi\nu(1 + 0.04K)}\right\}^{-1} & \text{for } r \leqslant r_p, \end{cases}\qquad(A14)$$

where ν is the disk gas viscosity given as $\nu = \alpha_{vis}c_sh_s$. To account for the disk depletion process, such as photoevaporation or disk wind, we set the disk depletion factor f_{dep} as

$$f_{dep} = \exp\left(-\frac{t}{\tau_{dep}}\right).\qquad(A15)$$

The surface density of disk gas at the gap bottom, which is used for the gas accretion rate and migration rate, is obtained as $\Sigma_{gap} = \Sigma_{gas}(r = r_p)$ using Equation (A8).

In our model, we set $\alpha_{vis} = 10^{-3}$, $M_{disk,0} = 0.1M_\odot$, and $R_{disk} = 200au$, respectively. The final orbital position of proto-Jupiter at the a_p–M_p plane is determined by the core formation time t_0 (e.g., Tanaka et al. 2020). We find that Jupiter stops at its current location due to the disk depletion if the core formed at $t_0 = 1.3 \times 10^6$ yr and $t_0 = 0.9 \times 10^6$ yr for Case 1 and Case 2, respectively. We continue the orbital integration for 1×10^7 yr. By the end of the simulation, we find that Jupiter does not grow further and that planetesimal accretion is negligible at that stage.

For the planetesimal disk, we assume that the planetesimal distribution follows the density profile of the gaseous disk at $t = 0$ and adopts the solid-to-gas ratio used in Turrini et al. (2021). To speed up the numerical simulation, we adopt the superparticles used in Shibata et al. (2021). We use 12,000 superparticles in Case 1 and 24,000 superparticles in Case 2. Superparticles are distributed from 3.9 to 8.4 au in Case 1 and from 3.9 to 23 au in Case 2. The initial eccentricity e and inclination i of planetesimals are given by the Rayleigh distribution, and we set $\langle e^2\rangle^{1/2} = 2\langle i^2\rangle^{1/2} = 10^{-3}$. The other orbital angles are distributed uniformly.

Figure 6 shows the disk model used in this Letter. The solid and dashed lines are the surface density of solid materials (or planetesimals) and gas, respectively. Figure 7 shows the evolution of the gas accretion timescale τ_{acc} (red) and the planetary migration timescale τ_{tide} (blue) in our model. The solid and dashed lines are the cases of $M_{th} = 10^{-2}$ and 10^{-3}, respectively. Both timescales rapidly increase around $M_p \sim M_J$ due to the exponential decay of disk gas. We stop our simulation at $t - t_0 = 1 \times 10^7$ yr. Even if we ran the simulation
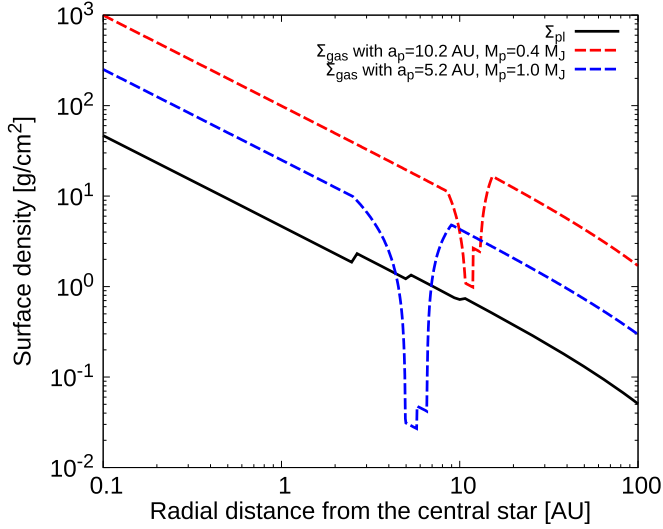
Figure 6. Disk profile used in our model. The solid line shows the planetesimal surface density profile. We adopt the solid-to-gas ratio used in Turrini et al. (2021). The dashed lines show the gas surface density profile when $M_p = 0.4 M_J$ (red line) and $M_p = 1.0 M_J$ (blue line) in Case 2.
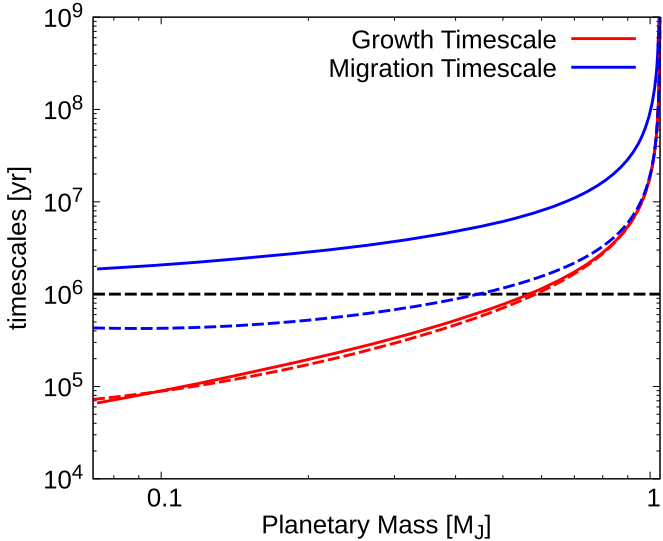
Figure 7. Evolution of timescales used in our model. The red and blue lines are the gas accretion timescale τ_{acc} and planetary migration timescale τ_{tide}, respectively. The solid and dashed lines are cases of $M_{th} = 10^{-2}$ and 10^{-3}, respectively. The dotted black line shows the depletion timescale $\tau_{dep} = 1 \times 10^6$ yr.

further, proto-Jupiter would no longer grow and migrate. When $M_{th} = 10^{-2}$, the fraction of timescales keeps a large value of $\tau_{tide}/\tau_{acc} \gg 1$. In this case, the planetary mass reaches Jupiter's mass before disk dissipation because τ_{acc} is smaller than/ comparable to the disk's depletion timescale τ_{dep}. However, the planet barely migrates because τ_{acc} is always longer than τ_{dep}. On the other hand, when $M_{th} = 10^{-3}$, the fraction of timescales decreases to ~ 1. Both timescales are smaller than or comparable to τ_{dep}, so proto-Jupiter can migrate over significant distances (~ 10 au) before the disk is dissipated.

In our simulations, planetesimal capture is considered to occur once a planetesimal enters proto-Jupiter's envelope. The

Table 1
Parameters Used in Our Simulations

M_s	Mass of Central Star	$1.0 M_\odot$	
$M_{disk,0}$	Initial mass of the proto-planetary disk	$0.1 M_\odot$	
R_{disk}	Typical size of the proto-planetary disk	200 au	
α	Disk viscosity parameter	1×10^{-3}	
τ_{dep}	Disk depletion timescale	1×10^6 yr	
$M_{p,0}$	Initial mass of the protoplanet	$6 \times 10^{-5} M_\odot$	
		in Case 1	in Case 2
$a_{p,0}$	Initial semimajor axis of the protoplanet	6.9 au	18.3au
t_0	Formation time of the planetary core	1.3×10^6 yr	0.9×10^6 yr

radius of proto-Jupiter is given by

$$R_p = \left(\frac{3 M_p}{4 \pi \rho_p} \right)^{1/3}, \qquad (A16)$$

where ρ_p is the mean density. During the detached phase, the planetary envelope is slightly expanded due to gas accretion (Valletta & Helled 2021). To include the effect, we set $\rho_p = 0.125$ g cm^{-3}. R_p in our model is always smaller than that obtained by Valletta & Helled (2021) by a factor of a few, and it is known that the capture radius is larger for smaller planetesimals (e.g., Inaba & Ikoma 2003). We do not expect significant differences if a more detailed calculation of the capture radius is considered. This could be explored in detail in future research. Table 1 shows the parameters used in this study.

Appendix B
The Effect of the Assumed Disk's Profile

In Section 3, we adopt a self-similar solution for a protoplanetary disk with $M_{disk,0} = 0.1 M_\odot$ and $R_{disk} = 200$ au. However, the structure and the size of protoplanetary disks are not well determined. Here, we show the results when assuming three different disk models. The first one is a small-disk model where we adopt the self-similar solution but with $M_{disk,0} = 0.03$ $M_\odot$ and $R_{disk} = 50a$ u. The second and third disk models are a steep-disk model and a flat-disk model where we adopt a simple disk profile given by

$$\Sigma_{Simple} = \Sigma_0 \left(\frac{r}{5.2 \text{ au}} \right)^{-\alpha_{disk}}, \qquad (B1)$$

with $\alpha_{disk} = 3/2$ for the steep disk and $\alpha_{disk} = 1/2$ for the flat disk. Σ_0 is set to 300 g cm^{-2} and the gap-opening factor, the gas accretion factor, and the disk depletion factor are adopted in the same way as in Equation (A8). Due to the different distribution of the disk gas, the evolution is different from the original model. However, the evolution pathways on the a_p-M_p plane are similar to the baseline model because the timescale fractions are independent of the disk's profile (see Equation (1)).

Figure 8 shows the results using the various disk models. The total captured mass of planetesimals and the timing of planetesimal accretion are similar to those of the baseline disk
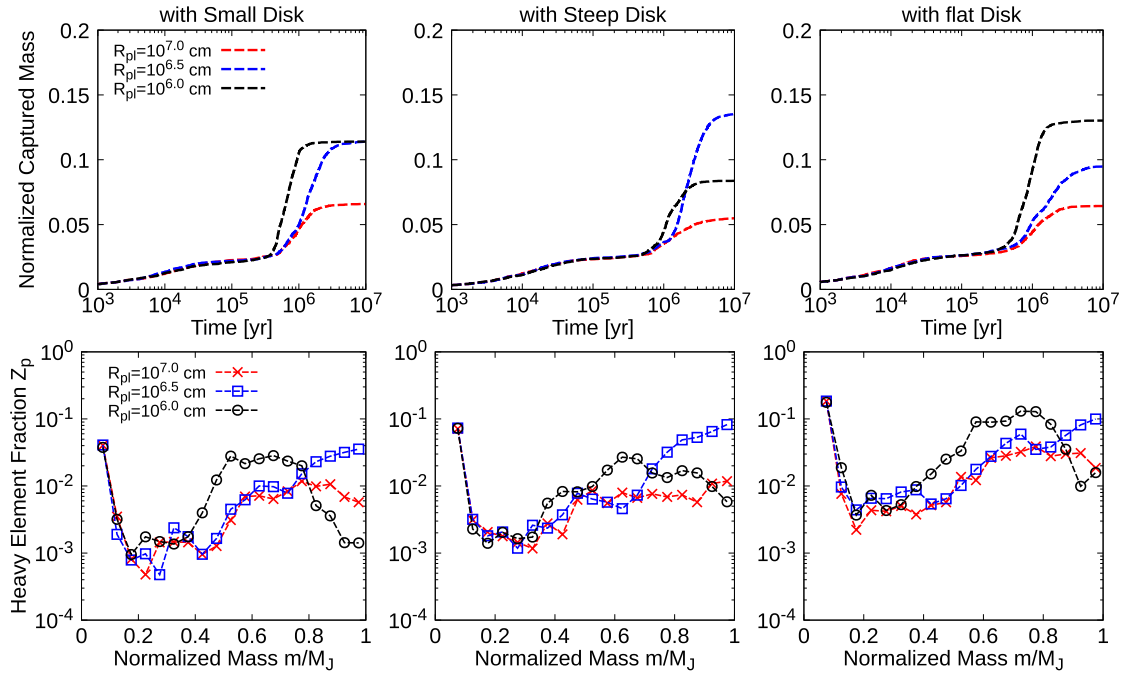
Figure 8. Same as Figure 2 but using a small-disk model (left), steep-disk model (middle), and flat-disk model (right). In the upper panels, we normalize the cumulative captured mass using the total solid mass used in each simulation. We adapt the evolution pathways of Case 2.

model. This is because the location of the SSP is nearly independent of the disk surface density profile (Shibata et al. 2021). Even if the gaseous disk had a different density distribution, the SSP would be located around Jupiter's orbit. Therefore, we conclude that the occurrence of a second planetesimal accretion phase where heavy elements are deposited into the upper envelope of proto-Jupiter is robust and does not depend on the assumed disk model.

Appendix C
Planetesimal Collisions

In our simulation, we adopt test particles for planetesimals and ignore collisions between planetesimals. As pointed out by Batygin (2015) and Shibata et al. (2021), planetesimal collisions could be important during the shepherding process. We find that more than 10 $M_\oplus$ of planetesimals are shepherded by the mean motion resonances before proto-Jupiter enters the SSP. These planetesimals could collide with each other as the planet migrates inwards. Once collisional cascade begins, the planetesimal size distribution can change and therefore affect (i.e., reduce) the planetesimal accretion rate.

The collision timescale depends on the total mass of the planetesimals shepherded by mean motion resonances. At the same time, the total mass shepherded by mean motion resonances changes with the planetesimal distribution. If the planetesimal disk is formed around the ice lines and has a ring-like distribution around 10–15 au, which is different from the uniform distribution used in our simulations, the total mass of planetesimals shepherded by mean motion resonances would be smaller than 10$M_\oplus$. In that case the collision timescale would be longer than the migration timescale and the second planetesimal accretion phase would start before the initiation of the collisional cascade (see Shibata et al. 2021 for further details). It is clear that the planetesimal distribution plays a key

role in this process and in some cases could prevent the initiation of the collisional cascade.

Appendix D
Effect of Other Planets

Our simulations focused on the interaction between a migrating planet and the surrounding planetesimals and do not include the existence of other protoplanets. The gravitational perturbations from other protoplanets, however, could affect the location of the SSP (Shibata et al. 2020). In addition, the migration of other planets can change the distribution of planetesimals and even contribute to further planetesimal formation (Shibaike & Alibert 2020). It is therefore clear that future studies should investigate formation pathways accounting for the growth of all the outer planets and their mutual interactions. Because the atmospheres of all outer planets in the solar system are measured to be enriched with heavy materials (e.g., Atreya et al. 2020), it is desirable to investigate planetesimal accretion mechanisms for all four planets.

ORCID iDs

Sho Shibata ● https://orcid.org/0000-0002-5418-6336
Ravit Helled ● https://orcid.org/0000-0001-5555-2652

References

Adachi, I., Hayashi, C., & Nakazawa, K. 1976, PThPh, 56, 1756
Alibert, Y., Mordasini, C., Benz, W., & Winisdoerffer, C. 2005, A&A, 434, 343
Andrews, S. M., Wilner, D. J., Hughes, A. M., Qi, C., & Dullemond, C. P. 2010, ApJ, 723, 1241
Armitage, P. J., Eisner, J. A., & Simon, J. B. 2016, ApJL, 828, L2
Asplund, M., Grevesse, N., Sauval, A. J., & Scott, P. 2009, ARA&A, 47, 481
Atreya, S. K., Hofstadter, M. H., In, J. H., et al. 2020, SSRv, 216, 18
Barnett, M. N., & Ciesla, F. J. 2022, ApJ, 925, 141
Batygin, K. 2015, MNRAS, 451, 2589

Bitsch, B., Izidoro, A., Johansen, A., et al. 2019, A&A, 623, A88
Bitsch, B., Lambrechts, M., & Johansen, A. 2015, A&A, 582, A112
Bosman, A. D., Cridland, A. J., & Miguel, Y. 2019, A&AS, 632, L11
Debras, F., & Chabrier, G. 2019, ApJ, 872, 100
Dones, L., Weissman, P. R., Levison, H. F., & Duncan, M. J. 2004, Comets II
    (Tucson, AZ: Univ. of Arizona Press)
Drążkowska, J., & Alibert, Y. 2017, A&AS, 608, A92
Eriksson, L. E. J., Ronnet, T., & Johansen, A. 2021, A&AS, 648, A112
Guillot, T., & Hueso, R. 2006, MNRAS, 367, L47
Guillot, T., Santos, N. C., Pont, F., et al. 2006, A&A, 453, L21
Guillot, T., Stevenson, D. J., Hubbard, W. B., & Saumon, D. 2004, Jupiter: The
    Planet, Satellites and Magnetosphere (Cambridge: Cambridge Univ.
    Press), 35
Helled, R., & Stevenson, D. 2017, ApJL, 840, L4
Hyodo, R., Guillot, T., Ida, S., Okuzumi, S., & Youdin, A. N. 2021, A&AS,
    646, A14
Ida, S., Tanaka, H., Johansen, A., Kanagawa, K. D., & Tanigawa, T. 2018,
    ApJ, 864, 77
Inaba, S., & Ikoma, M. 2003, A&A, 410, 711
Kanagawa, K. D., Tanaka, H., Muto, T., & Tanigawa, T. 2017, PASJ, 69, 69
Kanagawa, K. D., Tanaka, H., & Szuszkiewicz, E. 2018, ApJ, 861, 140
Kurokawa, H., & Tanigawa, T. 2018, MNRAS, 479, 635
Leconte, J., & Chabrier, G. 2013, NatGe, 6, 347
Li, C., Ingersoll, A., Bolton, S., et al. 2020, NatAs, 4, 609
Lichtenberg, T., Drążkowska, J., Schönbächler, M., Golabek, G. J., &
    Hands, T. O. 2021, Sci, 371, 365
Lozovsky, M., Helled, R., Rosenberg, E. D., & Bodenheimer, P. 2017, ApJ,
    836, 227
Lynden-Bell, D., & Pringle, J. E. 1974, MNRAS, 168, 603
Öberg, K. I., & Wordsworth, R. 2019, AJ, 158, 194
O'Brien, D. P., Morbidelli, A., & Bottke, W. F. 2007, Icar, 191, 434
Ohno, K., & Ueda, T. 2021, A&AS, 651, L2
Owen, T., Mahaffy, P., Niemann, H. B., et al. 1999, nat, 402, 269
Podolak, M., Haghighipour, N., Bodenheimer, P., Helled, R., & Podolak, E.
    2020, ApJ, 899, 45
Sasselov, D. D., & Lecar, M. 2000, ApJ, 528, 995
Schneider, A. D., & Bitsch, B. 2021, A&A, 654, 11
Shakura, N. I., & Sunyaev, R. A. 1973, A&A, 24, 337
Shibaike, Y., & Alibert, Y. 2020, A&AS, 644, A81
Shibata, S., Helled, R., & Ikoma, M. 2020, A&A, 633, 13
Shibata, S., Helled, R., & Ikoma, M. 2021, arXiv:2112.12623
Shibata, S., & Ikoma, M. 2019, MNRAS, 487, 4510
Shiraishi, M., & Ida, S. 2008, ApJ, 684, 1416
Stevenson, D. J. 1982, P&SS, 30, 755
Szulágyi, J., Masset, F., Lega, E., et al. 2016, MNRAS, 460, 2853
Tanaka, H., Murase, K., & Tanigawa, T. 2020, ApJ, 891, 143
Tanigawa, T., & Watanabe, S.-I. 2002, ApJ, 580, 506
Turrini, D., Schisano, E., Fonte, S., et al. 2021, ApJ, 909, 40
Valletta, C., & Helled, R. 2020, ApJ, 900, 133
Valletta, C., & Helled, R. 2021, MNRAS, 507, L62
Vazan, A., Helled, R., & Guillot, T. 2018, A&A, 610, 14
Venturini, J., & Helled, R. 2020, A&A, 634, A31
Wahl, S. M., Hubbard, W. B., Militzer, B., et al. 2017, GeoRL, 44, 4649
Wong, M. H., Mahaffy, P. R., Atreya, S. K., Niemann, H. B., & Owen, T. C.
    2004, Icar, 171, 105
Zhou, J., & Lin, D. N. C. 2007, ApJ, 666, 447